

Thunderclouds and accretion discs: a model for the spectral and temporal variability of Seyfert 1 galaxies

A. Merloni and A. C. Fabian

Institute of Astronomy, Madingley Road, Cambridge, CB3 0HA

ABSTRACT

X-ray observations of Seyfert 1 galaxies offer the unique possibility of observing spectral variability on timescales comparable to the dynamical time of the inner accretion flow. They typically show highly variable lightcurves, on a wide range of timescales, with Power Density Spectra characterized by ‘red noise’ and a break at low frequencies. On the other hand, time resolved spectral analysis have established that spectral variability on the shortest timescales is important in all these sources, with the spectra getting softer at high fluxes (in the 2-10 keV band, typically), while the reflection component and the iron line often exhibit a complex behaviour. Here we present a model that is able to explain a number of the above mentioned properties in terms of magnetic flares shining above a standard accretion disc and producing the X-ray spectrum via inverse Compton scattering of soft photons (both intrinsic and reprocessed thermal emission from the accretion disc and locally produced synchrotron radiation). We show that the fundamental heating event, likely caused by magnetic reconnection, must be compact, with typical size comparable to the accretion disc thickness and must be triggered at a height at least an order of magnitude larger than its size. The fundamental property of our ‘thundercloud’ model is that the spatial and temporal distribution of flares are not random: the heating of the corona proceed in correlated trains of events in an avalanche fashion. The amplitude of the avalanches obeys a power-law distribution and determines the size of the active regions where the spectrum is produced. Due to the feedback effect of the X-ray radiation reprocessed in the disc, larger active regions produce softer spectra. With our model we simulate X-ray lightcurves that reproduce the main observational properties of the Power Density Spectra and of the X-ray continuum short-term variability of Seyfert 1 galaxies. By comparing them with observations of MGC–6-30-15, we are able to infer that the accretion disc corona in this source must have a large optical depth ($\tau_T \gtrsim 1.5$) and small average covering fraction.

Key words: accretion, accretion discs - galaxies: active - galaxies: Seyfert - magnetic fields - radiation mechanisms: thermal - X-ray: general

1 INTRODUCTION

X-ray observations of accreting black holes, both in Seyfert 1 galaxies and in galactic sources (GBHC) typically show highly variable lightcurves, on a wide range of timescales. Time resolved spectral analysis have established that spectral variability on the shortest timescales is important in all these sources. For example, the analysis of average peak aligned shots of the GBHC Cygnus X-1 (Li, Feng & Chen 1999) has shown that, during the *hard* state and the transitions between the two states of the source, the spectrum evolves from hard to soft to hard again. Such kind of analysis, though, is much better suited for Active Galactic Nuclei (AGN). As a matter of fact, the dynamical timescale of a Keplerian accretion flow around a black hole, $t_{\text{dyn}} \simeq$

$9 \times 10^3 \varpi^{3/2} (M_{\text{BH}}/10^7 M_{\odot}) \text{ s}$ (where we have introduced the dimensionless radius $\varpi = R/R_S = c^2 R/2GM$), is such that it is much easier to perform reliable time resolved spectroscopy for the brightest AGN, where a typical flaring event may last hours or days.

There is in fact growing observational evidence for a number of Seyfert 1s, that during a flare the X-ray spectrum becomes softer as the 2-10 keV flux increases (see e.g. Done et al. (2000); Zdziarski & Grandi (2001); Petrucci et al. (2001a); Vaughan & Edelson (2001) and Nandra (2001) for a recent review). More recently, Georgantopoulos & Papadakis (2001) found similar trends in a number of Seyfert 2 galaxies observed with *RXTE*.

The analysis of the lightcurves in the frequency do-

main is usually presented in terms of Power Density Spectra (PDS). PDS of AGN are in general characterized by ‘red noise’ variability ($P(f) \propto f^{-\gamma}$, with $1 \lesssim \gamma \lesssim 2$) and a break at low frequencies (Lawrence & Papadakis 1993; Markowitz & Edelson 2001). Red noise is characteristic of many astrophysical systems (solar flares (Lu & Hamilton 1991), Soft Gamma Repeaters bursts (Gögüs et al. 1999), Gamma-ray bursts (Beloborodov et al. 2000; McBreen et al. 1994), etc.) as well as more familiar ones (tides, earthquakes and even radio broadcasting, see e.g. Press 1978; Montroll & Shlesinger 1982), and is intimately related to the turbulent and/or chaotic nature of such non-linear systems. Nevertheless, the information contained in the PDS alone is not enough to discriminate between different mechanisms that many authors have proposed as the origin of the $1/f$ noise.

In one of such attempts, Mineshige et al. (1994) (see also Mineshige & Negoro 1999) have proposed that black holes accretion flows develop into a state of Self-Organized Criticality (Bak, Tang & Wiesenfeld 1987) in which mass accretion occurs in avalanches, whose size is distributed as a power-law: large (and longer) shots contribute to the low-frequency part of the PDS, while small and shorter shots determine the power-law decline at high frequencies.

In general, in order to explain the observed values of γ in AGN and GBHC, any model requires individual signals of very different timescales. In this way Poutanen & Fabian (1999) were able to reproduce the properties of the observed Power Spectrum of the GBHC Cygnus X-1 using a simple stochastic pulse-avalanche model, originally proposed by Stern and Svensson (1996) to explain γ -ray burst temporal characteristics. In such model the individual signals correspond to coronal hard X-ray magnetic flares, which possess a range of durations and are capable to trigger larger avalanches.

Magnetic field reconnection of flux tubes in a tenuous corona is in principle capable of producing power-law distribution of active region sizes. In pioneering work, Tout & Pringle (1996) have demonstrated both with a simple analytic model and with Monte Carlo simulation, that, if a dynamo-generated magnetic field with a coherence scale of the order of the disc thickness emerges from the accretion disc, then the inverse cascade process of stochastic magnetic reconnection of flux tubes may lead to much larger coherent fields and active regions, with a power-law distribution in size.

Recently, Uttley & McHardy (2001) have discovered a remarkable linear correlation between RMS variability and flux in two X-ray binaries (Cygnus X-1 and the millisecond pulsar SAX J1808.4-3658). They have also found that the lightcurves of three Seyfert galaxies are consistent with such relationship and have therefore argued that such behaviour is an universal one in compact accreting systems.

Here we propose a simple model of Seyfert 1s high energy emission that combines the basic properties the accretion flows must have to reproduce the short timescales temporal and spectral characteristics of the observed objects.

The basic idea of our model is that magnetic reconnection in the accretion disc corona does not occur randomly in time and space, but rather in avalanches of correlated events (Poutanen & Fabian 1999). This not only affects the properties of the lightcurve, but, we argue, is responsible for the observed spectral variability. The spectrum produced in region

where a large number of heating events take place is different from the spectrum generated by an isolated event, as we discuss in the next section. Furthermore, large avalanches of magnetic flares may obscure the underlying disc as seen from the observer, and complicates the temporal behaviour of the secondary spectral features (reflection hump and fluorescent lines).

To build a full time-dependent model on the basis of the above ideas, including a detailed treatment of the radiative transfer in the accretion disc – corona system is undoubtedly a formidable task. Here we have chosen to simplify it by adopting an approximate analytic treatment for the spectral generation, following the works of Di Matteo, Celotti & Fabian (1997; 1999) and of Wardziński & Zdziarski (2000) (as discussed in Appendix A). This, we believe, gives a fair representation of the modeled system and enables us to highlight the main prediction of the model in the simplest possible way.

The paper is structured as follows: in the next section we outline the main features of our model, dealing separately with its spectral (section 2.1) and temporal (section 2.3) structure, and we elaborate on the thundercloud analogy (section 2.2). The results of numerical simulation and a discussion of the main physical consequences of the model are presented in sections 3 and 4, respectively. Finally, in section 5 we draw our conclusions.

2 MODEL OUTLINE

2.1 Structured coronae and thermal Comptonization

The best model to date that explains the spectra of Seyfert 1 galaxies is based on thermal Comptonization of soft photons in a hot electron cloud (Shapiro, Lightman & Eardley 1976; Sunyaev & Titarchuk 1980). Although it was early shown that the main features of the high-energy emission of black hole powered sources could be explained by the interplay of the hot cloud (the so-called *corona*) shining on a standard (optically thick, geometrically thin) accretion disc (Haardt & Maraschi 1991), the geometry of the hot and cold phases is still matter of debate. Such geometry could in principle be deduced with sufficient spectral information: for example, reflection features produced by a cold, optically thick medium illuminated by the hard X-ray power-law continuum are sensitive to the detail of the relative geometry of the two components (George & Fabian 1991; Matt, Perola & Piro 1991; Magdziarz & Zdziarski 1995). Simultaneous studies of UV (likely produced by thermal emission from the optically thick medium) and X-ray radiation have already been used in many cases to rule out a slab corona in favour of a patchy one, made of a number of separate active regions (Haardt, Maraschi & Ghisellini 1997; Stern et al. 1995; Di Matteo, Celotti & Fabian 1999), while the observed correlation between the photon index and the reflection strength (Zdziarski, Lubinski & Smith 1999; Gilfanov, Churazov, & Revnivtsev 2000) (which has been proved to hold on timescales much longer than the dynamical one) has demonstrated the need for a further geometrical/dynamical parameter, such as the relativistic bulk motion velocity of the coronal material (Beloborodov 1999a;

Malzac et al. 2001) and/or the truncation radius of the inner accretion disc (Zdziarski, Lubinski & Smith 1999).

As we focus here on short-term variability, we do not consider these latter possibilities (namely, we consider a *static* corona and a disc extending down to the innermost stable orbit) and assume that the X-ray spectrum is produced by thermal Comptonization in spherical active regions of size $R = rR_S$, lifted above the disc to a height $H = hR_S$ (Di Matteo, Celotti & Fabian 1999), and permeated by a magnetic field with intensity B . The seed photons for Comptonization are both synchrotron ones, produced locally by the interaction between the hot electrons and the magnetic field, and black-body ones coming from the underlying cold disc.

An active region illuminates the cold disc: part of the flux is reflected and part is absorbed and reprocessed. The geometry of the active region plays a crucial role in determining the comptonized spectrum: if $L(r)$ is the luminosity of an active region, we have for the reprocessed luminosity that returns to the active region and is comptonized there (Beloborodov 1999; Malzac, Beloborodov & Poutanen 2001)

$$L_{\text{rep}}(r) = L(r)(1 - a)(1 - \mu_0)/2, \quad (1)$$

where a is the disc albedo (that will be kept fixed to the value of 0.15 throughout the paper), and μ_0 is a geometric factor which regulates the feedback mechanism. As in Di Matteo, Celotti & Fabian (1999), we define a circular area of radius $R_{\text{hot}} = r_{\text{hot}}R_S$ in the accretion disc heated by an active region up to a temperature that depends on the illuminating flux, and define

$$\mu_0 = h/(r_{\text{hot}}^2 + h^2)^{1/2} \quad (2)$$

as the angular size of that circle measured from the center of the active region (at height h). As a typical relevant radius we take that one at which the temperature has decreased by a factor of 2, and we have $r_{\text{hot}} \simeq 2.3h + r$.

If most of the accretion power is dissipated in the corona, and the reprocessed radiation is the dominant source of soft photons for Comptonization, the ratio h/r determines the amplification factor, $A(r)$, and the active region temperature ($\Theta = kT_e/m_e c^2$): $A(r) = L/L_{\text{rep}} = 1 + 4\Theta + 16\Theta^2$. The resulting photon spectral index, Γ , can be related to A by the approximate expression (Beloborodov 1999a,b) $\Gamma \approx 2.33(A - 1)^{-\delta}$, where $\delta \approx 1/6$ for GBHC and $\delta \approx 1/10$ for AGNs. Clearly, for very large active regions ($h/r \rightarrow 0$), the amplification factor has a minimum and the spectrum is softer.

In the more general situation the dominant source of soft photons can be determined by comparing the local energy densities of the synchrotron radiation and of the thermal emission emerging from the disc, both from intrinsic dissipation and reprocessed radiation. As already discussed by Di Matteo, Celotti & Fabian (1997, 1999) and Wardziński & Zdziarski (2000), the relevance of synchrotron emission in a magnetically dominated active region decreases with increasing central source mass (so it is less important in AGN) and is a strong function of the temperature (the hotter the corona the more it is important). Therefore, in the coronal flow around an active galactic nucleus, synchrotron radiation is likely to be relevant only for very compact active regions (see Appendix A).

For each active region size r we calculate the spectrum

self-consistently: given an active region luminosity $L(r)$, we assume that the energy density of the magnetic field is in (almost) equipartition with that of the local radiation (Di Matteo, Celotti & Fabian 1997):

$$\frac{B^2}{8\pi} = \frac{3\epsilon_M L(r)t_0}{4\pi(rR_S)^3}, \quad (3)$$

where ϵ_M is the equipartition factor, of the order of unity, and $t_0(R) = R/v_{\text{diss}}$ is the dissipation time. The dissipation velocity v_{diss} depends on the uncertain nature of the heating process. For magnetic reconnection models it is related to the Alfvén speed v_A and to the magnetic Reynolds number R_m (which is very large in the low resistivity coronal plasma) and ranges from $v_A/\sqrt{R_m}$, in Sweet-Parker reconnection models (Sweet 1958; Parker 1979), to $v_A/\ln R_m$, in Petschek reconnection models (Petschek 1964). In the following (see section 2.3), on the basis of time variability argument, we will show that v_{diss} cannot be larger than a few percent of the speed of light, and discuss further how to constrain the dissipation time.

We calculate the self-absorbed synchrotron luminosity using the expression given in Wardziński & Zdziarski (2000); the intrinsic disc luminosity, instead, is simply given by $L_{\text{int}} = \dot{m}(1 - f_H)L_{\text{Edd}}$, where \dot{m} is the accretion rate in units of the Eddington one, f_H is the fraction of the accretion power dissipated in the corona (Svensson & Zdziarski 1994) and $L_{\text{Edd}} = 1.3 \times 10^{38} M/M_\odot$ is the Eddington luminosity. Finally, the reprocessed luminosity, $L_{\text{rep}}(r)$, is calculated from Eq. (1). The soft photon input flux from the accretion disc is then given by the sum of the two thermal components at different temperatures, the intrinsic and the reprocessed one (see Appendix A for details).

In the following calculations of our fiducial model we will fix the overall normalization constants $M_{\text{BH}} = 10^7 M_\odot$, $\dot{m} = 0.1$ and $f_H = 0.7$. Furthermore, we neglect radial dependence of the energy output and consider only the coronal flow above the inner, more luminous part of the accretion disc, so that $R_{\text{disc}} = 20R_S$.

To calculate the comptonized spectrum we use the analytic expression given in Wardziński & Zdziarski (2000) for a homogeneous and isotropic source characterized by optical depth τ_T and temperature Θ . To derive the emerging spectrum we fix the coronal optical depth, τ_T , the active region size r and its luminosity $L(r)$ (see section 2.2), and calculate the temperature by imposing that the total luminosity of the active region (synchrotron plus inverse Compton emission) equals $L(r)$ (as discussed in Appendix A).

In Fig. 1 we plot the coronal temperature, Θ , and the slope of the comptonized continuum, α , emerging from each active region as functions of an active region size, for different values of the optical depth. As anticipated, larger and more luminous regions are cooler, and henceforth softer, due to the larger reprocessed soft radiation they intercept. Although calculated for a spherical active region, for the sake of consistency we have checked that, in the limits $h/r \rightarrow \infty$ and $f_H \rightarrow 1$, our results agree with the prediction of Haardt & Maraschi (1993) for a slab corona in energy equilibrium above a cold accretion disc.

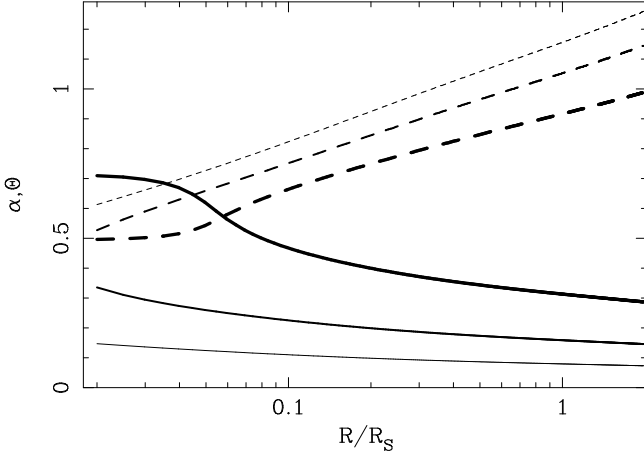


Figure 1. The equilibrium temperature ($\Theta = kT/m_e c^2$, solid lines) and spectral index $\alpha = \Gamma - 1$ (dashed lines) of an active region as a function of its size, for a fixed height $H = 1R_S$ and different optical depths, calculated for $C = 10^{-3}$ and $D = 1$ (see section 2.2). In order of decreasing line-thickness, the different curves correspond to $\tau_T = 0.5, 1, 2$. Due to the increased reprocessed radiation that is intercepted in the larger regions, the temperature drops with increasing r , and the emerging spectrum is softer. The shoulder at low values of R for the $\tau_T = 0.5$ case is due to the increased importance of synchrotron emission as a source of soft photons (see also Figure A1).

2.2 Active regions distribution and luminosity: the thundercloud analogy

In the hot, comptonizing corona the energy input is likely to be provided by a strong, highly intermittent magnetic field (see Merloni & Fabian 2001) amplified in the underlying turbulent disc by a dynamo process generated by the Magneto Rotational Instability (Balbus & Hawley 1998; Tout & Pringle 1992). Dissipation is then triggered by magnetic reconnection of flux tubes on the smallest possible scale (given approximately by the disk scaleheight). If these small reconnection sites were distributed randomly in time and space, all with a similar aspect ratio, h/r , we would observe shot-noise-like variability in the lightcurve and, more importantly, no spectral variability. If, on the other hand, the system is in some kind of critical state, such that each small flare can trigger an avalanche in its immediate neighborhood (i.e. the flares are spatially and temporally correlated), the situation will be qualitatively different. In fact, any such avalanche is effectively a large active region: more luminous (because it contains more reconnection sites), more extended and with a softer spectrum (because h/r is smaller, see previous section).

As a consequence of such avalanche generation process at any given time there would be a spread of active regions above the disc, with typical size ranging from the very small micro-flares ($R \sim$ disc scaleheight), to the larger avalanches ($R \sim$ a few Schwarzschild radii).

Hence, we assume that the luminosity of an active region is determined by the size of the avalanche, and therefore scale as the size of the region itself

$$L(r) = c_1 \dot{m} f_H L_{\text{Edd}} r^D. \quad (4)$$

Here D may be related to the spatial distribution of the

correlated flares (and be regarded as a fractal dimension of the reconnection sites) and/or to the radial dependence of the energy generation in the accretion disc.

On the other hand, because of the stochastic nature of the avalanche generation process, we will assume a *power-law* shape for the time-independent active region size distribution $n(r)$ (as also suggested by the shape of the observed power density spectra), such that the number of active regions of size r lying in the interval $(r, r + dr)$ is, *at any time*, given by

$$n(r)dr = c_2 r^{-p} dr. \quad (5)$$

The two constants c_1 and c_2 can be fixed imposing the over-all normalization for the total corona average covering fraction C and for the average hard luminosity:

$$C = \int_{r_{\min}}^{r_{\max}} n(r) \frac{A(r)}{A_{\text{disc}}} dr \quad (6)$$

$$L_{\text{hard}} = \dot{m} f_H L_{\text{Edd}} = \int_{r_{\min}}^{r_{\max}} n(r) L(r) dr, \quad (7)$$

where $A(r)$ is the area of the disc covered by an active region of size r and A_{disc} is the total area of the disc.

To summarize, we model the accretion disc corona as highly inhomogeneous stochastic system, whose basic building blocks, the active regions, can be viewed as ‘magnetic thunderclouds’, charged by the differential rotation of the underlying disc and/or the turbulent motions in the accretion flow. The sizes of the thunderclouds are distributed as a power-law. The fast energy release, triggered by magnetic reconnection on the smallest scales, heats progressively larger active regions. Each active region (thundercloud) produces the observed rapid flares (X-ray lightning strokes) by inverse Compton scattering soft photons coming mainly from the underlying optically thick accretion disc*. Furthermore, if the coronal optical depth τ_T is high enough, the active regions may obscure the X-ray spectral features produced in the cold disc (in particular the fluorescent lines and the reflection hump, as discussed in Matt, Fabian & Reynolds 1997 and Petrucci et al. 2001b, respectively) for an observer situated above them (and act therefore as ‘Compton clouds’).

2.3 Time variability and Power Density Spectra

In general, if the heating process is related to the dissipation of the magnetic field in the corona, the dissipation timescale is given by $t_0(R) \simeq 10^2 r M_7 b$ s, where $M_7 = M_{\text{BH}}/10^7 M_\odot$ and $b = c/v_{\text{dis}}$ (Haardt, Maraschi & Ghisellini 1994). Here we assume that the spectrum is produced instantaneously in

* It is interesting here to remark that the analogy between high energy astrophysical processes and terrestrial lightning is not new. McBreen et al. (1994) have pointed out the similarity between the log-normal properties of gamma-ray bursts lightcurves and those of terrestrial lightning. In the latter case, the durations, peak currents, intervals between the strokes in the flashes, and the flash charges are log-normally distributed (Berger et al. 1975). When the dispersion of a log-normal distribution is large, the distribution is mimicked by a $1/x$ distribution over a wide range of x , while it can be shown that amplification processes generally relate log-normally distributed variables to power-law tails (Montroll & Shlesinger 1982).

every active region, i.e. the timescale over which an active region is heated is longer than the region light-crossing time and $b \gtrsim$ a few. We fix $b = 30$ (see section 4.2 for a discussion of this point).

Power density spectra of both AGNs and GBHCs show a break that separates low-frequency white noise ($P(f) \sim \text{constant}$) from the red noise part of the PDS. Within our model, such a break can naturally be associated with the largest possible active region, and thus fix r_{max} . On the other hand, in any stochastic process in which the characteristic durations and amplitudes are distributed as power-laws, we have

$$N(t_0)I^2(t_0) \propto t_0^\beta \text{ for } t_{0,\text{min}} < t_0 < t_{0,\text{max}} \quad (8)$$

where $N(t_0)$ is the probability and $I^2(t_0)$ the mean square amplitude of a flare with a duration t_0 and the PDS is approximately given by

$$P(f) \propto f^{-\gamma} \quad \gamma = (3 + \beta), \quad (9)$$

in the range $(2\pi t_{0,\text{max}}) < f < (2\pi t_{0,\text{min}})$ (Lochner, Swank & Szymkowiak 1991). Then, according to our model, for which $N(t_0) \propto t_0^{-p}$ and $I(t_0) \propto t_0^D$, the observed slope of the PDS determines the relation between p and D :

$$p = 2D + 3 - \gamma. \quad (10)$$

In the following section we present a numerical simulation of the thundercloud model for AGN spectral/temporal variability, keeping fixed $\gamma = 1.5$ (as usually dictated by the observations of AGN), and we discuss the main observable consequences of the thundercloud model.

3 THE FULL PICTURE: RESULTS FROM SIMULATED LIGHTCURVES

In this section we describe the results we obtained from simulated lightcurves with variable X-ray spectra. To take into account time dependence we introduce a new distribution $n(r, t)$, defined in such a way that the number of active regions of size in the interval $(r, r + dr)$ generated in the time bin $(t, t + dt)$ is given by $n(r, t) dr dt$. In a stationary state $n(r, t)$ does not depend on t , and we assume $n(r) = n(r, t)t_0(r)$, where $t_0(r)$ is the total duration of an avalanche.

A simulated lightcurve (see Fig. 2 for an example) is then produced requiring that in any time bin the actual number $\mathcal{N}(r, t)$ of avalanches generated with size in the interval $(r, r + dr)$ be picked from a Poissonian distribution with mean $n(r, t)dr$ and then summing over all the active regions generated at any time. For the sake of simplicity we adopted a triangular shape for the individual flares profile. Because we enforce relation (10) for the indexes of the distribution, the final PDS has the correct slope in the red-noise part (see Figure 3).

The emerging spectrum is calculated superimposing the contribution from all the flaring regions active at that time. The photon index Γ is calculated for every time bin with a least square fit to the spectrum with a power-law model in the 3-10 keV band.

We have fixed $r_{\text{min}} = 0.02$ and $r_{\text{max}} = 4$. The average covering factor C , in turn, fixes the total number of active regions and the degree of variability (RMS) of the PDS.

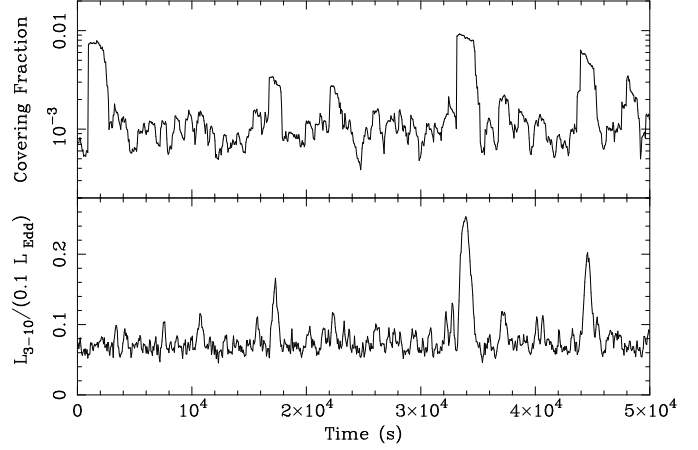


Figure 2. A simulated lightcurve (bottom panel) with its corresponding evolution of the covering fraction (top panel), for a $M_{\text{BH}} = 10^7 M_\odot$ central black hole accreting at one tenth of the Eddington rate.

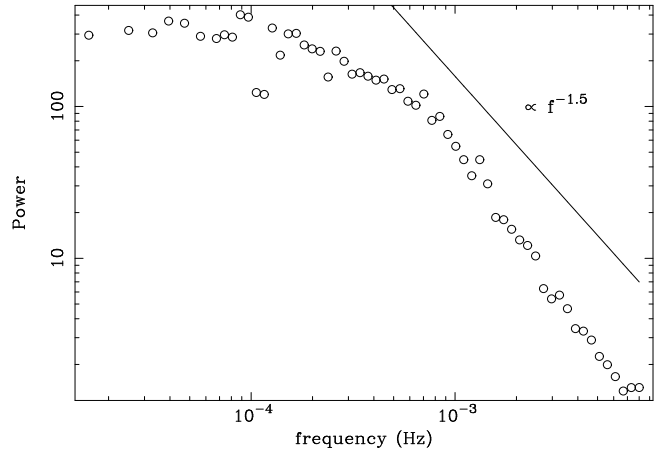


Figure 3. Power density spectrum of the simulated lightcurve shown in Fig. 2. The indexes of the active region distributions are $D = 1$ and $p = 3.5$. To reduce the scatter the PDS has been obtained averaging the power density spectra of 16 lightcurves of the total duration of 1.2×10^5 seconds each.

To explore the parameter space, we have simulated AGN light curves of total duration equal to 2.4×10^6 s, with a temporal resolution of 60 s. We varied the coronal optical depth (in the range $0.5 \leq \tau_T \leq 2$), the average covering fraction ($5 \times 10^{-4} \leq C \leq 2 \times 10^{-3}$) and the luminosity scaling index ($0.6 \leq D \leq 1.4$).

3.1 The spectral index-luminosity correlation

In Figure 4, for $D = 1$ and $C = 10^{-3}$, we plot the photon index Γ of the total emerging spectrum, measured in the 3–10 keV band, as a function of the luminosity in the same band, for three different values of the optical depth. As discussed in section 2, the higher the 3–10 keV luminosity, the softer the spectrum in that energy band, as observed. Furthermore, when the largest flares occur, and consequently the instantaneous covering fraction has a maximum (see Fig. 2), the $\Gamma - L$ relation tends to saturate to the softest value corresponding to an almost slab-like geometry. This is an intrinsic property of our model, and is due to the fact that larger active regions are cooler because the reprocessed soft luminosity that reenters the blobs (and is comptonized there) is larger.

Overall, we find a spectral variability range $\Delta\Gamma \sim 0.3 - 0.4$ for a change in luminosity of about a factor of four, similar to what is observed in many Seyfert 1s. It is worth remarking that a similar correlation was indeed predicted by Haardt, Maraschi & Ghisellini (1997) for the case of a pair dominated corona, but in that case the same $\Delta\Gamma$ was achieved for a luminosity variation of at least two orders of magnitude, which is clearly inconsistent with the observations. To verify that, we show in Figure 5 the observed $\Gamma - L$ correlation for the Seyfert 1 galaxy MCG–6–30–15 (from Vaughan & Edelson 2001) observed with *RXTE* in 1997[†].

For both our simulated lightcurves and the MCG–6 data we have fitted the Γ -luminosity relation with the function

$$\Gamma = \Gamma_0 - KL^\delta. \quad (11)$$

In Table 1 the values of the three fitting parameters Γ_0 , K and δ are listed for our set of simulated lightcurves. The asymptotic value of the photon index, Γ_0 , depends mainly on the optical depth, and is larger for larger values of τ_T . The exponent δ , instead, which determines the amount of spectral variation for a given increase in luminosity, is mainly dependent on the index D .

For the observed data plotted in Figure 5 we obtain $\Gamma_0 = 2.30^{+0.63}_{-0.02}$, $K = 6.8^{+20.8}_{-4.5}$ and $\delta = -1.31^{+0.79}_{-0.79}$. Compared to our model simulations, such a result is a strong indication of a relatively high value for the coronal optical depth ($\tau_T \gtrsim 1.5$) in this source, at least for the observation considered here. This, in turn, agrees well with the results presented in Guainazzi et al. (1999) of the analysis of a BeppoSAX observation of the same source: the measured spectral cut-off energy ($E_c \simeq 130 \pm 40$ keV for their best-fitting model), in the framework of thermal Comptonization models implies a coronal temperature[‡] $\Theta \sim 0.1$, that we ob-

[†] A thorough comparison of the thundercloud model with ASCA data for MCG–6–30–15 will be presented elsewhere (Shih et al. 2001).

[‡] We note that, usually, an e-folding power-law is not a good approximation for the actual shape of the observed high energy cut-off in many sources, in particular those with the better quality data, see e.g. Frontera et al. (2001). The actual coronal temperature is somewhat model and geometry dependent, and its real value for MCG–6–30–15 may differ from the one we adopt here by a factor of the order of unity, which does not change our main conclusion regarding the source optical depth.

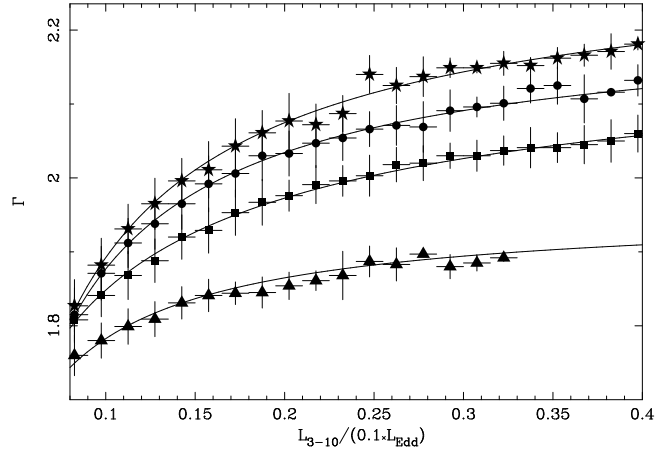


Figure 4. The observed photon index in the 3–10 keV band plotted versus the luminosity in the same band (in units of $0.1L_{\text{Edd}}$) as obtained from our fiducial simulation for $D = 1$ and $C = 10^{-3}$. The points for all the time intervals have been grouped in luminosity bins and the average gamma has been calculated. The error bars correspond to the weighted statistical uncertainty. Also shown are the best fitting functions (as in Table 1) for each of the four groups. Triangles corresponds to $\tau_T = 0.5$, squares to $\tau_T = 1$, circles to $\tau_T = 1.5$ and stars to $\tau_T = 2$.

tain for $\tau_T \gtrsim 1.5$ (see Fig. 1). Although it is more difficult to put tight constraints on the other two model parameters (D and C), nonetheless we may conclude that the observed $\Gamma - L$ correlation is consistent with $D \sim 1$ and $C \sim 10^{-3}$. Such a fairly small value for the average covering fraction is indeed required by the observed data: the smaller the covering fraction, the larger the observer variability, and the greater the chance of a large flare to occur. Too a large value of C would therefore drastically reduce the observed spectral variability. For our fiducial case, $D = 1$ and $C = 10^{-3}$, we have $c_1 = 0.16$ and $c_2 = 0.046$. The total number of active regions at any time is on average[§] $\mathcal{N} = \int n(r)dr \simeq 160$.

3.2 The variability-luminosity correlation

As already mentioned in the introduction, recent analysis of time variability properties of X-ray binaries and AGN (Uttley & McHardy 2001) have highlighted an intrinsic property of broadband noise variability in accreting compact objects, namely the strong linear correlation between RMS variability and flux.

We have analysed our simulated lightcurves to look for a similar correlation. With the parameters D and C fixed to the values of 1 and 0.001, respectively, we have simulated a lightcurve of the total duration of 4.3×10^6 s, subdivided it in 560 segments of 7680 s each in the first case, and in 2240 segments of 1920 s each in the second case, and calculated the mean luminosity and the variance σ for each segment in the standard way. The results, binned in luminosity intervals, are shown in Fig. 6. A clear correlation is evident in

[§] The total number of individual micro-flares that are the fundamental constituents of an avalanche is of course larger, depending on the actual number of events that are contained in any larger active region.

Table 1. Results from simulations and best fit parameters for the Γ -luminosity relation. We fitted a function of the form $\Gamma = \Gamma_0 - K L^\delta$.

Model parameters			Fit parameters		
C	D	τ_T	Γ_0	K	δ
0.0005	0.6	0.5	$2.01^{+0.04}_{-0.02}$	$0.050^{+0.041}_{-0.019}$	$-0.55^{+0.20}_{-0.20}$
0.0005	0.6	1.0	$2.21^{+0.11}_{-0.04}$	$0.08^{+0.12}_{-0.03}$	$-0.49^{+0.23}_{-0.22}$
0.0005	0.6	1.5	$2.30^{+0.01}_{-0.02}$	$0.058^{+0.019}_{-0.013}$	$-0.65^{+0.11}_{-0.11}$
0.0005	0.6	2.0	$2.34^{+0.01}_{-0.01}$	$0.030^{+0.011}_{-0.008}$	$-0.93^{+0.13}_{-0.14}$
0.0005	1.0	0.5	$2.07^{+0.01}_{-0.02}$	$0.11^{+0.45}_{-0.07}$	$-0.37^{+0.23}_{-0.41}$
0.0005	1.0	1.0	$2.21^{+0.18}_{-0.06}$	$0.10^{+0.25}_{-0.05}$	$-0.56^{+0.26}_{-0.26}$
0.0005	1.0	1.5	$2.32^{+0.13}_{-0.05}$	$0.10^{+0.01}_{-0.003}$	$-0.62^{+0.22}_{-0.22}$
0.0005	1.0	2.0	$2.32^{+0.01}_{-0.01}$	$0.040^{+0.013}_{-0.009}$	$-1.00^{+0.11}_{-0.12}$
0.0005	1.4	0.5	$1.96^{+0.01}_{-0.01}$	$0.019^{+0.072}_{-0.009}$	$-0.89^{+0.68}_{-0.92}$
0.0005	1.4	1.0	$2.09^{+0.01}_{-0.01}$	$0.010^{+0.012}_{-0.009}$	$-1.28^{+0.63}_{-0.64}$
0.0005	1.4	1.5	$2.15^{+0.35}_{-0.05}$	$0.085^{+0.43}_{-0.005}$	$-1.44^{+1.22}_{-1.70}$
0.0005	1.4	2.0	$2.38^{+0.02}_{-0.02}$	$0.070^{+0.01}_{-0.003}$	$-0.81^{+0.50}_{-0.79}$
0.001	0.6	0.5	$2.09^{+0.31}_{-0.07}$	$0.13^{+0.30}_{-0.05}$	$-0.35^{+0.22}_{-0.22}$
0.001	0.6	1.0	$2.20^{+0.10}_{-0.05}$	$0.075^{+0.096}_{-0.035}$	$-0.62^{+0.24}_{-0.24}$
0.001	0.6	1.5	$2.36^{+0.05}_{-0.06}$	$0.13^{+0.05}_{-0.005}$	$-0.46^{+0.10}_{-0.19}$
0.001	0.6	2.0	$2.36^{+0.05}_{-0.02}$	$0.081^{+0.052}_{-0.030}$	$-0.63^{+0.15}_{-0.16}$
0.001	1.0	0.5	$1.96^{+0.02}_{-0.01}$	$0.024^{+0.003}_{-0.005}$	$-0.88^{+0.77}_{-0.76}$
0.001	1.0	1.0	$2.21^{+0.34}_{-0.05}$	$0.11^{+0.06}_{-0.02}$	$-0.54^{+0.30}_{-0.31}$
0.001	1.0	1.5	$2.23^{+0.02}_{-0.02}$	$0.048^{+0.030}_{-0.022}$	$-0.86^{+0.49}_{-0.48}$
0.001	1.0	2.0	$2.32^{+0.14}_{-0.08}$	$0.071^{+0.15}_{-0.046}$	$-0.79^{+0.29}_{-0.30}$
0.001	1.4	0.5	$2.04^{+0.08}_{-0.03}$	$0.019^{+0.072}_{-0.009}$	$-0.89^{+0.68}_{-0.92}$
0.001	1.4	1.0	$2.17^{+0.01}_{-0.02}$	$0.010^{+0.012}_{-0.009}$	$-1.28^{+0.63}_{-0.64}$
0.001	1.4	1.5	$2.22^{+0.09}_{-0.09}$	$0.085^{+0.43}_{-0.005}$	$-1.44^{+1.22}_{-1.70}$
0.001	1.4	2.0	$2.34^{+1.43}_{-0.16}$	$0.057^{+0.051}_{-1.196}$	$-0.85^{+0.70}_{-0.72}$
0.002	0.6	0.5	$1.92^{+0.02}_{-0.02}$	$0.0011^{+0.001}_{-0.0005}$	$-2.1^{+0.3}_{-0.4}$
0.002	0.6	1.0	$2.17^{+0.14}_{-0.05}$	$0.077^{+0.133}_{-0.042}$	$-0.63^{+0.29}_{-0.29}$
0.002	0.6	1.5	$2.32^{+0.01}_{-0.01}$	$0.13^{+0.03}_{-0.01}$	$-0.52^{+0.71}_{-0.67}$
0.002	0.6	2.0	$2.39^{+0.14}_{-0.06}$	$0.11^{+0.13}_{-0.04}$	$-0.61^{+0.22}_{-0.22}$
0.002	1.0	0.5	$1.96^{+0.07}_{-0.02}$	$0.010^{+0.006}_{-0.003}$	$-1.19^{+0.59}_{-0.62}$
0.002	1.0	1.0	$2.11^{+0.03}_{-0.01}$	$0.006^{+0.002}_{-0.001}$	$-1.6^{+0.40}_{-0.40}$
0.002	1.0	1.5	$2.17^{+0.11}_{-0.04}$	$0.016^{+0.001}_{-0.0005}$	$-1.26^{+0.58}_{-0.59}$
0.002	1.0	2.0	$2.67^{+0.35}_{-0.14}$	$0.29^{+0.35}_{-0.12}$	$-0.43^{+0.19}_{-0.19}$
0.002	1.4	0.5	$1.92^{+0.05}_{-0.03}$	$0.015^{+0.035}_{-0.014}$	$-1.21^{+0.68}_{-0.69}$
0.002	1.4	1.0	$2.01^{+0.02}_{-0.01}$	$0.002^{+0.001}_{-0.004}$	$-1.75^{+0.76}_{-0.70}$
0.002	1.4	1.5	$2.46^{+1.21}_{-0.16}$	$0.21^{+0.92}_{-0.05}$	$-0.43^{+0.32}_{-0.30}$
0.002	1.4	2.0	$2.21^{+0.17}_{-0.06}$	$0.025^{+0.096}_{-0.018}$	$-1.04^{+0.45}_{-0.46}$

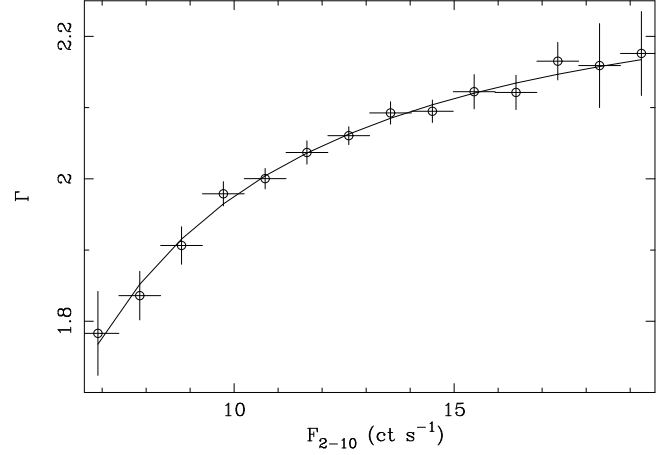


Figure 5. The observed photon index in the 2-10 keV band plotted versus the RXTE count rate in the same band for the Seyfert 1 galaxy MCG-6-30-15, from the analysis of Vaughan & Edelson (2001) (their Figure 3). The data point have been grouped in flux bins and the errors correspond to the weighted statistical uncertainty on the value of the spectral index. Also shown is the best fitting function of the form $\Gamma = \Gamma_0 - K F^\delta$. We obtain $\Gamma_0 = 2.30^{+0.63}_{-0.02}$, $K = 6.8^{+20.8}_{-4.5}$ and $\delta = -1.31^{+0.79}_{-0.79}$.

both cases, consistent with a linear one. We fitted a function of the form $\sigma = k(L_{3-10} - L_0)$, with k and L_0 constants, and found $k = 1.49 \pm 0.05$ and $L_0 = 0.091 \pm 0.006$ for the long interval case (dashed line in Fig. 6), and $k = 1.11 \pm 0.04$ and $L_0 = 0.063 \pm 0.005$ for the short interval case (solid line in Fig. 6). In the framework of the thundercloud model such behaviour can be explained by the non-random nature of the flare distribution. In fact, the large number of small, hard, low luminosity active regions constitutes a roughly constant background, with very low RMS variability, while much higher variability is associated with the rare large luminous events. The different slopes of the correlation in the two cases simply reflect the fact that the length of the segments in which we subdivided the lightcurve is shorter than the longest flare timescale, and we are sampling the PDS in its red-noise part.

4 DISCUSSION

4.1 Coronal scaleheight

In the above calculation we have kept fixed the value of the height of the flares above the accretion disc. In fact, as long as the main source of soft photons for Comptonization is the reprocessed radiation from the disc itself (as in the case of our fiducial model for which $c_r > c_i \gg c_s$, see Appendix A), what matters for the spectral properties of the source is the ratio h/r of an active region height over its size. Then, in order for the model to accommodate spectral variations as large as those observed in many Seyfert 1 galaxies, we need $r_{\min} \ll h \ll r_{\max}$.

If the small-scale flux loops are generated by a self-sustaining magnetic dynamo operating inside the disc, it is natural to identify the size of the smallest active regions emerging from the disc, i.e. the micro-flares that trigger the larger avalanches, with the accretion disc thickness (Tout

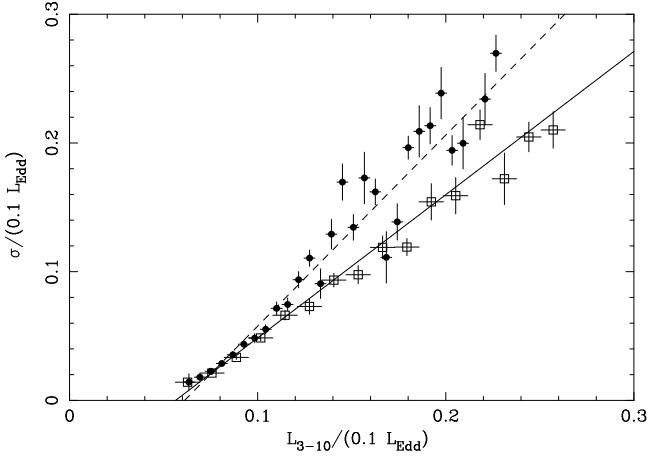


Figure 6. Luminosity dependence of the variance calculated for segments of a simulated lightcurve ($D = 1$, $C = 10^{-3}$ and $\tau_T = 1$) 7.7×10^3 (filled circles, dashed best fitting line) and 1.9×10^3 (open squares, solid best fitting line) seconds long, with resolution of 60 seconds. The fitting functions are of the form $\sigma = k(L_{3-10} - L_0)$, with k and L_0 constants.

& Pringle 1996; Galeev, Rosner & Vaiana 1979; Nayakshin & Kazanas 2001). Thus, the observed spectral variability implies that the average elevation of a reconnection site is larger (and perhaps much larger) than the disc scaleheight, as firstly proposed by Di Matteo (1998).

It is interesting that full MHD simulations of magneto rotational instability in weakly magnetized accretion discs indeed show the formation of a strongly magnetized corona, considerably more extended in the vertical direction than the disc itself (Miller & Stone 2000). Moreover, in the framework of a model similar to the one we present here, Di Matteo, Celotti & Fabian (1999) studied observations of the GBHC GX 339-4 in different spectral states to place limits on the model parameters, and in particular on the flare height. They conclude that the X-ray emission from galactic black holes in their *hard* state is more likely a result of inverse Compton scattering of soft photons in hot magnetic flares triggered high above the accretion disc.

The analytic treatment of Svensson & Zdziarski (1994) of the accretion disc–corona system allows us to give an estimate of the ratio of the coronal to disc scaleheight in the inner, radiation pressure dominated, part of the disc. From such a calculation, we can conclude that indeed, given the observed coronal temperatures, whenever most of the accretion power is released in the corona (say, $f_H \gtrsim 0.7$), the corona is much more extended in the vertical direction than the underlying disc. We have

$$\frac{H_c}{H_d} = \left(\frac{m_e}{m_p}\right)^{1/2} \frac{4}{9} \varpi^{3/2} \Theta^{1/2} \dot{m}^{-1} J(\varpi)^{-1} (1 - f_H)^{-1} \\ \gtrsim 16 \left(\frac{\Theta}{0.1}\right)^{1/2} \left(\frac{\dot{m}}{0.1}\right)^{-1} \left(\frac{(1 - f_H)}{0.1}\right)^{-1}, \quad (12)$$

where ϖ is the radial disc coordinate in units of Schwarzschild radii, $J(\varpi) = 1 - \sqrt{3/\varpi}$, and the last inequality is obtained taking the minimum of $\varpi^{3/2}/J(\varpi)$.

In the case of a structured corona the situation ought to be more complicated: if the flux tubes emerging from the disc carry a magnetic field with strength comparable to the

equipartition with the internal disc pressure, they will tend to expand (reducing the strength of the magnetic field) in the less pressurized coronal atmosphere (Parker, 1979, §8.4). However, if the flux tubes are twisted, as is likely to be the case if they are anchored in the differentially rotating disc underneath, their sideways expansion is counterbalanced by the generation inside the flux tube itself of an azimuthal field component, with a net increase of its total magnetic energy content. The flux rope will rise buoyantly (Parker, 1979, §9.1, 9.6), keeping a much lower aspect ratio (defined as the ratio of the loop length over its diameter). To conclude, given the major uncertainties on the magnetic flux tube dynamics in the disc–corona interface, we believe that it is not unlikely for the height of the magnetic flares in the corona to be larger than the disc thickness[¶], as envisaged in our model, and, indeed, needed to explain the large observed spectral variability.

4.2 The magnetic field

Within the framework of active coronal models for the hard X-ray emission of black hole accretion flows, the exact nature of the heating process remains the most elusive issue. Here, following the argument of Merloni & Fabian (2001), we have assumed that the magnetic field is the main repository of the energy in the corona and that the active regions are heated by the dissipation of such energy, probably via magnetic reconnection.

Although there is a growing consensus on the dynamical importance of magnetic fields in accretion discs, mainly driven by recent progresses in numerical MHD simulation of accretion flows and magneto–rotational instability, the detailed topology of the magnetic field is far beyond the reach of our current theoretical understanding. The solar analogy has provided theorists with ideas and inspiration, if not with quantitative insight, but it is wise to bear in mind that although we are able to actually image magnetic structures in our nearest star, even the heating of the solar corona is still not well understood.

With these *caveats* in mind, we discuss here some of the implications of our stochastic model for the accretion disc corona on the strength of the magnetic field and on the heating mechanism.

The ratio of magnetic to thermal energy in an active region is given by

$$E_{\text{mag}}/E_{\text{th}} \simeq \frac{\epsilon_M c_1 r^D \dot{m} f_H L_{\text{Edd}} t_0 \sigma_T}{4\pi \tau_T R^2 k T_e} \\ \sim 1.3 \times 10^3 \frac{\epsilon_M \dot{m} f_H b}{\tau_T \Theta} c_1 r^{D-1}. \quad (13)$$

For the standard set of physical parameters we have adopted, as long as the energy in the magnetic field is more than a few percent of the equipartition with the emitted radiation field, we have $E_{\text{mag}} \sim 25 r^{D-1} E_{\text{th}}$ and the active

[¶] As a final remark, we note that a puzzling characteristic of solar coronal loops, so often invoked in analogy with accretion disc coronal ones, is their tendency to have a nearly uniform thickness, instead of being substantially wider at their tops than at their foot-points, as expected from a straightforward application of the force-free assumption (Klimchuk, Antiochos & Norton, 2000).

regions are indeed magnetically dominated. In fact, the magnetic field intensity can be estimated as

$$B \simeq 1.6 \times 10^4 \tau_T^{1/2} r^{(D-1.5)} M_7^{-1/2} \left(\frac{b}{30}\right)^{1/2} \text{ G}. \quad (14)$$

Furthermore, we have $v_A/c \simeq 0.03 r^{D-1} b^{1/2}$. This translates into $v_A/c \simeq 0.1 r^{2(D-1)/3} (\ln R_m)^{1/3}$, in the case of Petschek-type reconnection (see section 2.1). It is evident that the slow Sweet-Parker reconnection model is not compatible with the above scenario, because it would lead to too large a magnetic field accumulated in the corona. Our adopted value of the parameter b , is instead more appropriate for a relatively fast reconnection, as in the Petschek-type model. In principle the value of such a parameter could be inferred from temporal studies, if we independently knew the physical characteristic size of an emitting region, as its value affects primarily the timescale of the individual flares.

To conclude, as already discussed in section 2, we would like to remark on the fact that synchrotron radiation is hardly important as source of seed photons for Comptonization in AGN, but for the hardest, compact short lived flares. However, direct synchrotron light at frequencies near the self-absorption cut-off could be observed below the peak of the disc quasi-thermal hump in sources where the direct emission from the accretion disc is strongly suppressed (i.e. for low accretion rates, high fraction of power dissipated in the corona and/or high relativistic bulk motion of the corona itself).

4.3 Iron line variability

The X-ray spectra of accreting black holes, and those of Seyfert 1s in particular, often show a clear sign of reflected radiation in the form of a prominent fluorescent iron $K\alpha$ line. This spectral component is sensitive to the geometry of the disc-corona system and can be then used to place more firm constraints on it. Often such lines are Doppler and gravitationally broadened, suggesting that the cold material within which they are produced is moving at relativistic speeds in the deep potential well of the central black hole (Fabian et al. 2000). In the standard picture in which the reflection features are produced by the accretion disc illuminated by the hard X-rays coming from the active regions, the strong observed continuum variability should drive the line variability with a short time-lag.

This simple picture, though, is challenged by the observations, which seem to indicate that, although the iron line does indeed vary with the varying flux, its flux is not correlated with the changes of the continuum intensity or of its slope (Vaughan & Edelson 2001).

In the framework of the thundercloud model, such complicated behaviour can be explained by the fact that the observed line at any time is the super-position of different features produced by active regions illuminating the disc with different spectral shape and intensity. The ionization properties of the surface of the accretion disc, which in turn determine the line characteristics, are strongly dependent on the illuminating continuum properties (Nayakshin, Kazanas & Kallman 2000; Done & Nayakshin 2001; Ballantyne, Ross & Fabian 2001; Ballantyne 2001). Therefore the observed iron line is expected to be complex, and variable on a wide range of timescales in a complicated way.

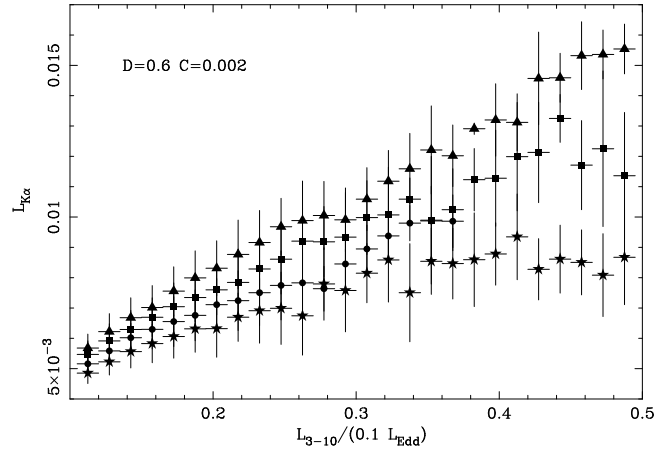


Figure 7. The estimated iron line luminosity, as calculated in Eq. (15) as a function of the observed flux in the 3-10 keV band (in units of $0.1 L_{\text{Edd}}$) for the simulation with $D = 0.6$ and $C = 0.002$. The points for all the time intervals have been grouped in luminosity bins and the average line flux has been calculated. The error bars correspond to the weighted statistical uncertainty. Triangles corresponds to $\tau_T = 0.5$, squares to $\tau_T = 1$, circles to $\tau_T = 1.5$ and stars to $\tau_T = 2$.

Furthermore, as the coronal optical depth becomes larger the reflection features are strongly suppressed by Compton scattering in the corona itself (Matt et al. 1997; Petrucci et al. 2001b). This effect becomes more important the larger is the active region. Analogously to what discussed in Malzac et al. (2001), we define a geometrical parameter that determines the fraction of reflected luminosity that reenters an active region, $\mu_s = h / \sqrt{4r^2 + h^2}$. Therefore, we can quantify the effect of an obscuring thundercloud by estimating the iron $K\alpha$ line luminosity produced by any given illuminating spectrum of an active region in the following way:

$$L_{K\alpha} = (L_{7-20}/2) a [\mu_s + (1 - \mu_s)(1 - P_{\text{sc}}(\tau_T))], \quad (15)$$

where $L_{7-20}/2$ is the luminosity above the iron $K\alpha$ edge emitted towards the disc and P_{sc} is the scattering probability in an active region (see Appendix A). A fraction μ_s of the reflected X-rays reaches the observed directly, while a fraction $(1 - \mu_s)P_{\text{sc}}$ suffers further Compton scattering in the corona and is therefore scattered out of the line, reducing its absolute flux. We note here that the above expression may be in fact underestimating the amount of cloud obscuration because the optical depth τ_T that enters in the determination of P_{sc} is the one calculated from the center of an active region and is smaller than that seen by the photons coming from the underlying disc.

In Figure 7 we show the estimated total Fe $K\alpha$ line luminosity produced by all the simultaneous active regions for a simulation with $C = 0.001$ and $D = 1$, plotted as a function of the total observed 3-10 keV luminosity. Clearly, in the case of high coronal optical depth ($\tau_T \gtrsim 1.5$), although still mildly correlated with the observed continuum at low luminosity (small flares and small timescales), the line variability is strongly suppressed at high luminosity (larger flares and longer timescales), to the extent that for a variation of a factor of three in the 3-10 keV flux, the line flux may increase only by about 50%.

In general, even for less dramatic cases, we expect the line equivalent width $W_{K\alpha}$ to decrease with the increasing flux. For example, in the simulation presented in Fig. 7, for $\tau = 1.5$, we have $W_{K\alpha} \sim 300\text{eV}$ for $L_{3-10} \simeq 0.1$ and $W_{K\alpha} \sim 200\text{eV}$ for $L_{3-10} \simeq 0.3$. Such a high value for the unattenuated iron line equivalent width (compared to the expected value of $\sim 100\text{ eV}$; George & Fabian 1991) can be consistent with a static corona model if the iron is overabundant with respect to the solar value, as indeed has been shown to be required to explain the reflection features of MCG-6-30-15 (Lee et al. 2000).

A full simulation of the temporal behaviour of the iron line, which is clearly beyond the scope of this work, will involve a full treatment of the ionization state of the accretion disc atmosphere below different active regions (with different illuminating spectra) and of the obscuring effects of the corona itself. Similarly, the effect of Comptonization in the corona on the shape and intensity of the reflection hump may reveal themselves in time-resolved spectral analysis of the hard X-ray emission, though this may prove a difficult task for the existing instruments capabilities (Petrucci et al. 2001b).

5 CONCLUSION

We have presented a model for spectral and temporal variability of the X-ray emission from accretion disc coronae around black holes. We have assumed thermal Comptonization as the main radiation mechanism to produce the observed X-ray continuum. The cooling radiation comes either from the intrinsic dissipation of gravitational energy in the underlying accretion disc, or from the reprocessed radiation in the cold disc or from synchrotron radiation produced locally in the magnetically dominated corona. For the case of a typical AGN of $10^7 M_\odot$, accreting at ten percent of the Eddington ratio and for which most of the power is dissipated in the corona ($f_H \gtrsim 0.7$), we have shown that the reprocessed radiation is usually the main source of soft photons but from the case of more compact and hot active regions, where the contribution from synchrotron radiation is important. Nonetheless, the magnetic field in the corona acts as the main energy reservoir and dominates the local energy budget.

The basic geometric properties of the coronal flow assumed in our model and, we believe, required to explain the observed spectral and temporal variability of AGN are the following:

- The corona must not be uniform, but structured and heated intermittently (Merloni & Fabian 2001);
- The fundamental heating event, a flare likely caused by magnetic reconnection, must be compact, with typical size comparable to the accretion disc thickness;
- The height of the reconnection site must be at least an order of magnitude larger than its size;
- The spatial and temporal distribution of the flares are not random, but proceed in correlated trains of events in an avalanche fashion;
- The size of the avalanches determines the size of the active regions and their luminosity, and are distributed as a power-law.

We have simulated X-ray lightcurves of AGN and studied the correlation between the photon index and the X-ray luminosity. By comparing our simulations with observation of the best studied Seyfert 1 galaxy MCG-6-30-15 we conclude that the model is able to reproduce the observed Γ -luminosity correlation and to put some constraints on the model parameter. In particular, to explain the trend observed in the 1997 *RXTE* observations analysed by Vaughan & Edelson (2001) we need a fairly high coronal optical depth ($\tau_T \gtrsim 1.5$), a small *average* covering fraction ($\sim 10^{-3}$) and a scaling index for the active region luminosity $D \sim 1$. Furthermore our model naturally explains the linear correlation between luminosity and RMS variability (at different epochs in the same source), recently discovered by Uttley & McHardy (2001) in a number of accretion-powered compact objects.

Our model does not include other important geometrical or dynamical parameters that may vary on timescales much longer than that over which the corona is heated (which is close to the dynamical one) and may indeed be relevant to determine the average long-term spectral properties of these sources. In fact, our model does not reproduce the observed correlation between the spectral index and the reflection features (Zdziarski, Lubinski & Smith 1999; Lubinski & Zdziarski 2001), and no ‘static’ corona does, as demonstrated by Malzac et al. (2001). If the corona instead is in stable relativistic bulk motion (i.e. is the base of a jet/outflow), and the outflow velocity changes with time, or from source to source, then we expect the average spectral index to correlate with the amount of reflection (Beloborodov 1999a; Malzac, Beloborodov & Poutanen 2001), as observed. Then our model would be applicable as it is only to the sources with the softest spectra (and indeed the spectral parameters of MCG-6-30-15 correspond to negligible bulk coronal velocity in the model of Beloborodov 1999a).

On the other hand, such a correlation has not yet been proved to hold on the short timescales we focused our attention on. The short-time variability should bear information on some fundamental properties of any accreting system in which an optically thick and geometrically thin disc coexist with a hot Comptonizing medium heated by dissipation of a structured magnetic field. A dynamic corona, where the reconnection sites moves with relativistic velocities and generate an outflow whose global properties evolve on timescales much longer than the dynamical one, is a straightforward generalization of the thundercloud model we have presented here, and should be considered in order to better constrain the geometry and dynamics of the inner accretion flow around black holes.

Thus, detailed analysis of time-averaged spectra will help determining the value of the parameter that is ultimately responsible for the long-term variability and therefore for the Γ -R correlation (such as the bulk outflow velocity, for example), while spectral and temporal variability on short timescales will ultimately probe the physics of coronal heating and magnetic reconnection, providing a test for the model we have illustrated in this work.

ACKNOWLEDGMENTS

We thank the referee, Dr. Andrzej Zdziarski, for the useful comments and suggestions. We thank Simon Vaughan for the MGC-6-30-15 data and for fruitful discussion, together with David Shih, Kazushi Iwasawa and David Ballantyne. This work was done in the research network “Accretion onto black holes, compact stars and protostars” funded by the European Commission under contract number ERBFMRX-CT98-0195’. AM and ACF thank the PPARC and the Royal Society for support, respectively.

REFERENCES

- Bak P., Tang C. & Wiesenfeld K., 1987, Phys. Rev. Lett., 59, 381.
 Balbus S. A. & Hawley J. F., 1998, Rev. Mod. Phys. 70, 1.
 Ballantyne D. R., Ross R. R. & Fabian A. C., 2001, MNRAS in press. astro-ph/0102040
 Ballantyne D. R., 2001, submitted to MNRAS.
 Beloborodov A. M., 1999a, ApJ, 510, L123.
 Beloborodov A. M., 1999b, in ‘High Energy Processes in Accreting Black Holes’, ASP Conference Series 161, ed. J. Poutanen & R. Svensson p.295.
 Beloborodov A. M., Stern B. E. & Svensson R., 2000, ApJ, 535, 158.
 Berger K., Anderson R. B. & Kröninger H., 1975, Electra, 80, 23.
 Di Matteo T., 1998, MNRAS, 299, L15.
 Di Matteo T., Celotti A. & Fabian A. C., 1997, MNRAS, 291, 805.
 Di Matteo T., Celotti A. & Fabian A. C., 1999, MNRAS, 304, 809.
 Done C., Madejski G. M., Zycki P. T., 2000, ApJ, 536, 213.
 Done C. & Nayakshin S., 2001, ApJ, 546, 41.
 Fabian A. C., Iwasawa K., Reynolds C. S. & Young A. J., 2000, PASP, 112, 1145.
 Frontera et al., 2001, ApJ, in press. astro-ph/0107199.
 Galeev A. A., Rosner R. & Vaiana G. S., 1979, ApJ, 229, 318.
 Georgantopoulos I. & Papadakis I. E., 2001, MNRAS, 322, 218.
 George I. M. & Fabian A. C., 1991, MNRAS, 249, 352.
 Gilfanov, M., Churazov, E., & Revnivtsev, M. 2000, to appear in Proc. of the 5th CAS/MPG Workshop on High Energy Astrophysics. astro-ph/0002415.
 Göğüs E., Woods P. M., Kouveliotou C., van Paradijs J., Briggs M. S., Duncan R. C., Thompson C., 1999, ApJ, 526, 93.
 Guainazzi M. et al., 1999, A&A, 341, L27.
 Haardt F. & Maraschi L., 1991, ApJ, 380, L51.
 Haardt F., Maraschi L. & Ghisellini G., 1994, ApJ, 432, L95.
 Klimchuk J. A., Antiochos S. K. & Norton D., 2000, ApJ, 542, 504.
 Lawrence A. & Papadakis I., 1993, ApJ, 414, L85.
 Lee J. C., Fabian A. C., Brandt W. N., Reynolds C. S., Iwasawa K., 1999, MNRAS, 310, 973.
 Lee J. C., Fabian A. C., Reynolds C. S., Brandt W. N., Iwasawa K., 2000, MNRAS, 318, 857.
 Li T. P., Feng Y. X. & Chen L., 1999, ApJ, 521, 789.
 Lochner J. C., Swank J. H. & Szymkowiak A. E., 1991, ApJ, 376, 295.
 Lu E. T. & Hamilton R. J., 1991, 1991, ApJ, 380, L89.
 Lubiński, P. & Zdziarski, A. A. 2001, MNRAS, 323, L37.
 Magdziarz P. & Zdziarski A. A., 1995, MNRAS, 273, 837.
 Malzac J., Beloborodov A. & Poutanen J., 2001, MNRAS, in press. astro-ph/0102490
 Markowitz A. & Edelson R., 2001, ApJ, 547, 684.
 Matt G., Perola G. C. & Piro L., 1991, A&A, 247, 25.
 Matt G., Fabian, A. C. & Reynolds, C. S., 1997, MNRAS, 289, 175.
 McBreen B., Hurley K. J., Long R. & Metcalfe L., 1994, ApJ, 271, 662.
 Merloni A. & Fabian A. C., 2001, MNRAS, 321, 549.
 Miller K. & Stone J. M., 2000, ApJ, 534, 398.
 Mineshige S., Takeuchi M. & Nishimori H., 1994, ApJ, 435, L125.
 Mineshige S. & Negoro H., 1999, in ‘High Energy Processes in Accreting Black Holes’, ASP Conference Series 161, ed. J. Poutanen & R. Svensson p.113.
 Montroll E. W. & Shlesinger M. F., 1982, Proc. Nat. Acad. Sci., 79, 3380.
 Nandra K., 2001, to appear in Advances in Space Research. astro-ph/0012448.
 Nayakshin S., Kazanas D. & Kallman T. R., 2000, ApJ, 537, 833.
 Nayakshin S. & Kazanas D., 2001, submitted to ApJ. astro-ph/0101312
 Osterbrock, D. E., 1974, *Astrophysics of gaseous nebulae*. W. H. Freeman and Co.
 Parker E. N., 1979, *Cosmical magnetic fields*. Clarendon Press, Oxford.
 Petrucci et al., 2001a, to appear in Proc. of “X-ray astronomy 2000”, (Palermo, Sep. 2000), Eds. R. Giacconi, L. Stella, S. Serio, ASP Conf. Series, in press.
 Petrucci P.-O., Merloni A., Fabian A. C., Haardt F. & Gallo E., 2001b, submitted to MNRAS.
 Petschek H. E., 1964, AAS-NASA Symp. on Physics of Solar Flares, NASA SP-50, p. 425.
 Press W. H. 1978, Comm. Astrophys., 7, 103.
 Poutanen J. & Fabian A., 1999, MNRAS, 306, L31.
 Shapiro S. L., Lightman A. P. & Eardley, D. M., 1976, ApJ, 204, 187.
 Shih D. et al., 2001, in preparation.
 Stern B. E., Begelman M. C., Sikora M. & Svensson R., 1995, MNRAS, 272, 291.
 Stern B. E. & Svensson R., 1996, ApJ, 469, L109.
 Sunayev R. A. & Titarchuk L. G., 1980, A&A, 86, 121.
 Svensson R. & Zdziarski A. A., 1994, ApJ, 436, 599.
 Sweet P. A., 1958, in Proc. IAU Symp. 6, Electromagnetic Processes in Cosmical Physics. Camb. Univ. Press, p. 123.
 Tout C. A. & Pringle J. E., 1992, MNRAS, 259, 604.
 Tout C. A. & Pringle J. E., 1996, MNRAS, 281, 219.
 Uttley P. & McHardy I. M., 2001, To appear in MNRAS. astro-ph/0103367.
 Vaughan S. & Edelson R., 2001, ApJ, 548, 694.
 Wardziński G. & Zdziarski A. A., 2000, MNRAS, 314, 183.
 Zdziarski A. A., 1985, ApJ, 289, 514.
 Zdziarski A. A., 1986, ApJ, 303, 94.
 Zdziarski A. A. & Grandi P., 2001, ApJ, 551, 186.
 Zdziarski, A. A., Lubiński, P. & Smith, D. A. 1999, MNRAS, 303, L11.

APPENDIX A: THE X-RAY SPECTRUM

We calculate the self-absorbed synchrotron luminosity using the expression given in Wardziński & Zdziarski (2000). The intrinsic disc luminosity is simply $L_{\text{int}} = \dot{m}(1 - f_{\text{H}})L_{\text{Edd}}$, where \dot{m} is the accretion rate in units of the Eddington one, f_{H} is the fraction of the accretion power dissipated in the corona (Svensson & Zdziarski 1994) and $L_{\text{Edd}} = 1.3 \times 10^{38} M/M_{\odot}$ is the Eddington luminosity. Finally, the reprocessed luminosity, $L_{\text{rep}}(r)$, is calculated from Eq. (1). For the two corresponding thermal soft photon fluxes from the disc $F_{\text{bb},i}$ and $F_{\text{bb},r}$, we assume black-body spectra, with temperatures Θ_i and Θ_r , respectively. They are given by:

$$\Theta_i = \left(\frac{k}{m_e c^2} \right) \left(\frac{L_{\text{int}}}{\sigma_B 4\pi R_{\text{disc}}^2} \right)^{1/4} \quad (\text{A1})$$

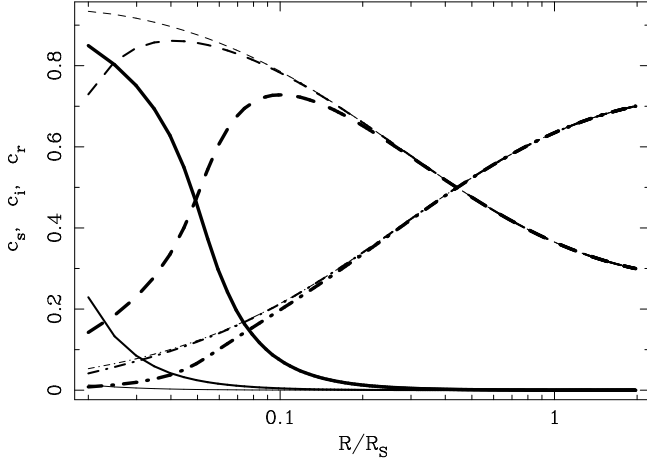


Figure A1. The relative contribution to the cooling luminosity from synchrotron radiation (c_s , solid lines), intrinsic dissipation in the accretion disc (c_i , dashed lines) and from reprocessed radiation (c_r , dot-dashed lines), as functions of an active region size r for $D = 1$ and a covering fraction of 10^{-3} . The energy densities are calculated for a fixed height above the disc $H = 1R_S$ in the case of an AGN with $M_{BH} = 10^7 M_\odot$ accreting with $\dot{m} = 0.1$, $f_H = 0.7$ and $\epsilon_M = 0.1$. The thickness of the lines indicates the optical depth: in order of decreasing thickness we have $\tau_T = 0.5, 1, 2$. Clearly synchrotron radiation is important only for the more compact sources with the lowest optical depth, which are hotter and produce harder spectra, as shown also in Figure 1. Reprocessed radiation energy density, instead, always dominates as a source of soft photons for Comptonization for large enough active regions. Such behaviour is common for all values of the parameters; as a rule, the reprocessed radiation is more important for smaller covering fraction and higher values of the fraction of power dissipated in the corona f_H .

$$\Theta_r = \left(\frac{k}{m_e c^2} \right) \left(\frac{L_{\text{rep}}(r)}{\sigma_B 4\pi R_{\text{hot}}^2} \right)^{1/4}. \quad (\text{A2})$$

Comparing the energy densities of the three photon fields inside each active region, we determine the coefficients c_s , c_i and c_r , with $c_s + c_i + c_r = 1$, that fix the relative contribution of synchrotron, intrinsic and reprocessed soft photons sources, respectively. This is illustrated in Fig. A1 for our fiducial model parameters and $\epsilon_M = 0.1$. It is evident that for $r \gtrsim 0.1h$ the contribution of synchrotron radiation to the cooling luminosity is always negligible, in particular for the high optical depth (lower temperature) cases.

The luminosity due to the scattered photons can be approximated as a sum of a cut-off power-law and Wien component (Wardziński & Zdziarski 2000),

$$L_C = N_P \left(\frac{x}{\Theta} \right)^{-\alpha} \exp^{-x/\Theta} + N_W \left(\frac{x}{\Theta} \right)^3 \exp^{-x/\Theta}, \quad (\text{A3})$$

where $x = h\nu/m_e c^2$ is a dimensionless photon energy, N_P and N_W are the normalizations of the power-law and Wien tail, respectively, and are related by the ratio (Zdziarski 1985)

$$\frac{N_W}{N_P} = \frac{\Gamma_E(\alpha)}{\Gamma_E(2\alpha + 3)} P_{\text{sc}}, \quad (\text{A4})$$

where $\Gamma_E(x)$ is Euler's Gamma function.

The scattering probability averaged over the source vol-

ume, P_{sc} , depends on the coronal optical depth only, and determine the emerging spectral index:

$$\alpha = -\frac{\ln P_{\text{sc}}}{\ln A}. \quad (\text{A5})$$

In spherical geometry (Osterbrock 1974),

$$P_{\text{sc}} = 1 - \frac{3}{8\tau_T^3} [2\tau_T^2 - 1 + \exp^{-2\tau_T}(2\tau_T + 1)]. \quad (\text{A6})$$

Finally, we have for the power-law normalization

$$N_P = 4\pi r^2 \phi \left[c_i F_{\text{bb},i}(\Theta_i) \left(\frac{2.78\Theta_i}{\Theta} \right)^\alpha + c_r F_{\text{bb},r}(\Theta_r) \left(\frac{2.78\Theta_r}{\Theta} \right)^\alpha + c_s F_s \left(\frac{x_t}{\Theta} \right)^\alpha \right] \quad (\text{A7})$$

where the synchrotron flux $F_s = 2\pi m_e c^3 \Theta x_t^2 / \lambda_c^3$ and x_t is the turnover energy (in units of $m_e c^2$) of the self-absorbed synchrotron radiation, that has been calculated as in Di Matteo Celotti & Fabian (1997). The factor $\phi \approx (1 + 4\Theta^2)/(1 + 40\Theta^2)$ approximates the relative normalization of the power-law extrapolation and the soft photon input peak flux, and is derived from a phenomenological analysis (Zdziarski 1986).

The coronal temperature, and consequently the slope of the comptonized continuum emerging from each active region, are calculated self-consistently solving for $L_C = L(r) = c_1 \dot{m} f_H L_{\text{Edd}} r^D$.

This paper has been produced using the Royal Astronomical Society/Blackwell Science L^AT_EX style file.